Efficient and Robust Power Management of Reduced Cost Distributed Power Electronics for Fuel-Cell Power System

Sudip K. Mazumder[1]
Associate Professor
Department of Electrical and Computer Engineering,
Director of the Laboratory of Energy and Switching-Electronics System,
University of Illinois at Chicago,
851 South Morgan Street,
1020 SEO,
M/C 154,
Chicago, IL 60607
e-mail: mazumder@ece.uic.edu

Sanjaya Pradhan
Design Engineer
Philips Lighting,
10275 W. Higgins Road,
Rosemont, IL 60018
e-mail: sanjaya.k.pradhan@philips.com

Batteries in a fuel-cell power system are essential to providing the additional power during the sharp load-transients. This necessitates a power-electronics subsystem (PES), which controls the energy flow between the fuel-cell stack, the battery, and the application load during the transient and in the steady states. In this paper, a distributed PES (comprising a multimodule dc-dc boost converter) is proposed for a fuel-cell and battery based hybrid power system, which provides higher cost effectiveness, efficiency, and footprint savings. This is realized by interfacing both the fuel-cell stack and the battery to the distributed PES using transfer switches, which are so controlled such that during a load transient, power from both the battery power and the fuel-cell stack is fed to the load via the PES while the stack energy input is adjusted for the new load demand. During the steady-state, the control implements a dynamic-power-management strategy such that only an optimal number of power converter modules of the distributed PES are activated yielding improved optimal energy-conversion efficiency and performance. Furthermore, using a composite Lyapunov-method-based methodology, the effect of dynamic change in the number of active power converter modules with varying load conditions on the stability of the PES is also outlined. Finally, the PES concept is experimentally validated by interfacing a multimodule bidirectional dc-dc boost converter with Nexa® proton exchange membrane (PEM) fuel-cell stacks from Ballard Power Systems.
[DOI: 10.1115/1.3119059]

Keywords: dc-dc converter, fuel cell, battery, power management, control, PEM, efficiency, power electronics, stability

1 Introduction

Fuel-cell based power system is comprised of a fuel-cell-stack subsystem (FCSS), a balance-of-plant subsystem (BOPS) that controls the flow rate of fuel and air to the FCSS and maintains the temperature of the stack, and a power-electronics subsystem (PES) that provides the power interface between the FCSS and application load(s). The slow response time of the BOPS mechanical system as compared with the electrochemical and electrical time constants of the fuel-cell and the PES has been a major concern for fuel-cell power system designers [1–4]. During a sudden increase in the load demand, the fuel utilization increases rapidly [3] and several works are in progress to enhance the response time of the BOPS to mitigate this problem that can have degrading effect on the performance of the cell [5]. However, currently, the most widely used approach is the use of an energy-buffering device (e.g., a battery), which provides the additional energy to the load during the load transient, thereby preventing a sudden change in stack power flow. However, for energy buffering, an energy-management system is necessary to control the energy flow between the energy generator (fuel-cell stack) and the storage device (battery) and the application load during the transient and steady states.

Several researchers are working on this issue related to the control of the fuel-cell/battery based hybrid energy-management system. A control system is proposed in Ref. [6], which controls the state-of-the charge (SOC) of the battery by manipulating the voltage of the stack via the dynamic system modeling of predetermined parameters for the stack and the battery. This control strategy tries to eliminate the need for any input power converter, resulting in the cost reduction in the power system. However, this strategy neither provides any option to alleviate the degrading effects of the load transient on the stack nor it considers the efficiency of the power system. A fuel-cell/battery hybrid energy-management system with microprocessor-based control is proposed in Ref. [7], which attempts to alleviate the degrading effects of the load transients by enabling the fuel-cell stack to be taken out of the system when the load requirement exceeds a fixed maximum energy output of the stack. Because the efficiency and the energy density of the battery are small as compared with the fuel-cell stack, at higher loads (when the battery needs to supply increasingly larger current) the efficiency of the system goes down. As such, the required energy storage capacity of the battery increases, leading to an increase in the space and cost of the battery and the power system.

In some of the prior works for the design of fuel-cell hybrid energy-management system only one power converter was used either at the output of the battery or the stack. For instance in Refs. [8,9], a dc-dc converter is connected at the stack output to deliver a more stable output voltage to the load while the battery is connected at the converter output. However, during a load transient, battery handles the full-load current until the battery voltage goes below the bus voltage, which leads to an oscillation. Moreover, uncontrolled charging may damage the battery. Finally, as the required bus voltage increases, the number of batteries required to support the higher bus will also increase, leading to higher cost of the system.

In another approach [10], the power system uses a power con-

[1]Corresponding author.
Manuscript received January 24, 2008; final manuscript received August 9, 2008; published online November 11, 2009. Review conducted by Nigel M. Sammes.

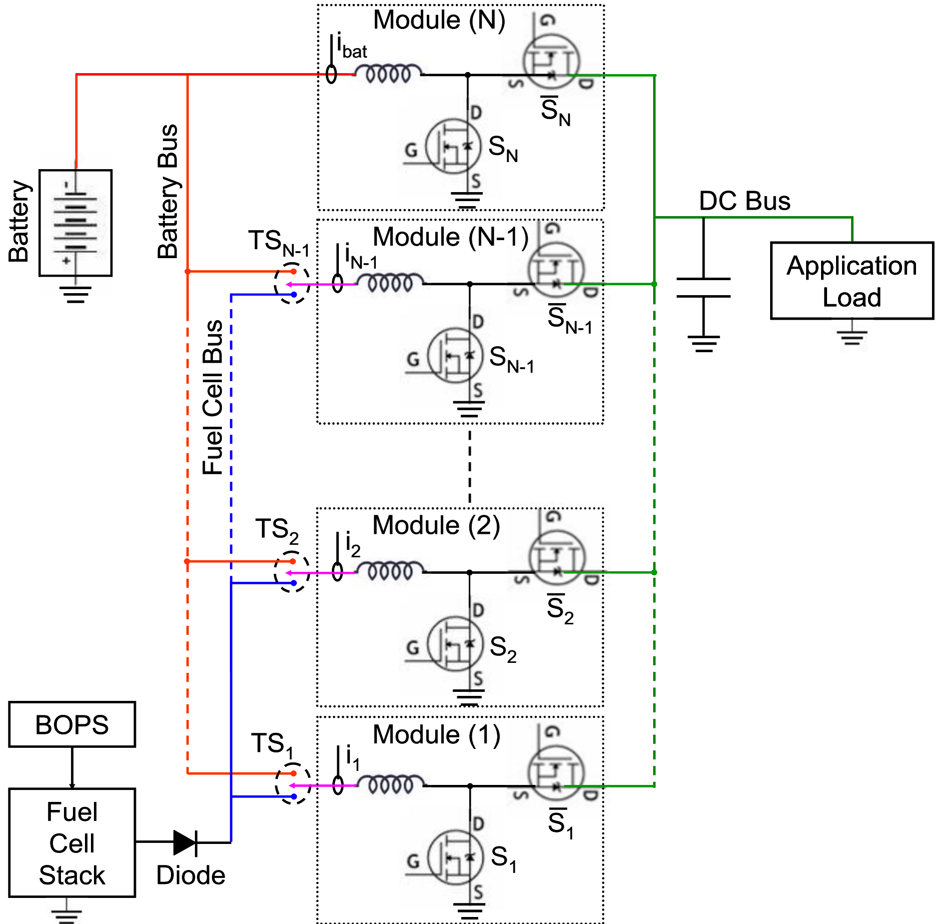

Fig. 1 Topology of the distributed PES comprising *N* dc-dc power-converter modules (with primary MOSFET switches S_1 through S_N and their complementary counterparts) along with $N-1$ transfer switches ($TS_1 - TS_{N-1}$)

verter to control the power flow from the battery, which provides additional power to the load when the stack voltage goes below a certain minimum. However, as experimentally investigated in this work, the battery current does not respond to an abrupt load increase immediately and hence cannot prevent the zero-reactant condition in the stack unless the operating fuel utilization is inefficiently low.

The dual-power-converter approach used by Jang et al. [11] avoids the limitations of the aforementioned approaches. However, with either the battery or the stack able to provide the full-load power independently, the converter redundancy of the system is 2 that leads to higher cost, footprint space, and weight of the power system. Finally, in an effort to reduce the PES redundancy, Kambouris and Bates [12] used an insulated-gate bipolar transistor (IGBT) six-pack to implement three bidirectional dc-dc converters to control the power from the battery and the fuel cell. The bidirectional converters are connected selectively to the battery and/or the fuel-cell stack based on the load demand and the fuel-cell-stack capability. However, this approach is not suitable for the mitigation of the load-transient since the stack and the battery are in series. Furthermore, the architecture is not modular and hence, not suitable for higher power.

To address the pending challenges outlined above, a power-management control system for a distributed PES (comprising multiple modules of dc-dc boost converters) for a fuel-cell power system is outlined in this paper. The distributed PES serves as the power-electronic interface for both the fuel-cell stack as well as the battery, thereby reducing the cost of the PES as well as its weight and footprint space. This, in turn, alleviates the high cost of the fuel-cell power system, which is currently one of the bottlenecks with regard to the commercialization of such systems. Moreover, due to the dynamic-power-management of the modules of the distributed PES, the shortcoming of conventional PES (with regard to typical characteristics of drooping efficiency with reducing output power) is alleviated. This, in turn, optimizes the performance and efficiency of the overall power system while nullifying the effects of load transients on the fuel-cell stack. Furthermore, using a composite-Lyapunov-function-based methodology, the stability of the PES undergoing dynamic change in the number of active power converter modules with varying load conditions is formulated. Finally, validation of the PES concept is outlined by interfacing a multimodule bidirectional dc-dc boost converter with Nexa proton exchange membrane (PEM) fuel-cell stacks from Ballard Power Systems.

2 Description of the PES and Control System

Figure 1 shows the topology of the distributed PES, which interfaces to the fuel-cell stack and the battery. It consists of multiple bidirectional dc-dc (boost) converter modules. The number of these modules (N) depends on the maximum load demand and the rated capacity of the individual converter modules. Assuming that the rated power of the individual converter is P_{rated} and the maximum overall power demand of the load (including battery charging) is $P_{\max}$, the total number of the modules (N) is given by $N=\mathrm{ceil}(P_{\max}/P_{\mathrm{rated}})+1$, where the ceil function returns the smallest integer, greater than the fraction $P_{\max}/P_{\mathrm{rated}}$. Furthermore, the redundancy of the distributed-PES architecture is given by

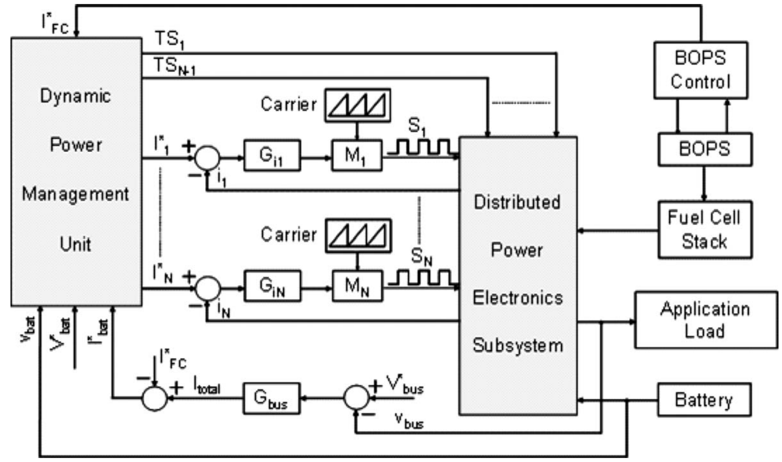

Fig. 2 DPMU for the PES to realize optimal energy-conversion efficiency and transient ride-through. Symbols G_{bus} and G_{i1} through G_{iN} represent the bus-voltage compensator and the current-loop compensators (for the N dc-dc converter modules). Only m ($\leq N-1$) modules are active at any time while the rest of the ($N-1-m$) modules are turned off. The Nth module is always connected to the battery. Each of the $N-1$ transfer switches ($TS_1 \ldots TS_{N-1}$) also receives input from the DPMU.

$N/(P_{max}/P_{rated}) \approx N/N-1$. The outputs of all the modules are connected in parallel to a bus capacitor while the inputs of the $N-1$ modules are connected (using transfer switches TS_1 through TS_{N-1}) to either the fuel-cell stack or the battery depending on the load demand and the operating efficiency. A dedicated bidirectional (Nth) converter is connected directly to the battery to facilitate the charging of the battery even when the power system is delivering full power to the load. It is noted that, for part-load operation, other modules of the PES can be used for charging the battery as well.

Figure 2 shows the control-system architecture for the distributed PES. The BOPS controller outlined in Ref. [13] generates the stack reference current I^*_{FC}. The linear bus-voltage-error compensator (G_{bus}), outlined in Ref. [13], generates the total current reference I_{total} by comparing the bus-voltage reference with feedback bus-voltage. The difference between I_{total} and I^*_{FC} is the required battery current reference I^*_{bat}. Subsequently, using I^*_{FC} and I^*_{bat}, the dynamic-power-management unit (DPMU) generates the transfer switch signals and the current references I^*_1 through I^*_N that is fed to the inner current loops for generating switching signals for the converters.

The dynamic-power-management strategy is as follows. In the *steady-state*, when the load demand is met by the fuel-cell stack, the DPMU determines the number of dc-dc converter modules ($m \leq N-1$) to be connected to the fuel-cell stack and the module current reference signals I^*_1 through I^*_m to ensure optimal power sharing that will maximize the overall efficiency of the distributed PES. *The optimal condition for this efficient power strategy is described in Sec. 2.1*. Furthermore, the DPMU uses the battery voltage (v_{bat}) and its set point (V^*_{bat}) as inputs and controls the charging current to the battery (provided by the fuel-cell stack) using the Nth dedicated dc-dc converter with a current reference of I^*_N ($=I^*_{bat}$). To enhance the response of the bidirectional dc-dc boost converters, current-mode control is used for the PES, which is based on the control of the input current for the desired output bus voltage. The PES control, using the outputs of the linear compensators G_{i1} through G_{im} and G_{iN}, generates the switching signals S_1 through S_m and S_N using the modulators M_1 through M_m and M_N for the m active converter modules and the dedicated Nth converter. The structure of the jth current-loop compensator is represented by the transfer function $G_{ij}(s)=K_{ij}(1+s/\omega_{zij})/s(1+s/\omega_{pij})$. The compensator structure for the voltage-loop compensator is the same as well, that is, $G_{bus}(s)=K_v(1+s/\omega_{zv})/s(1+s/\omega_{pv})$. The choice of the gains and placements of the poles and zeros are described in Ref. [13]. The DPMU also generates the on/off signals for the transfer switches $TS_1 \ldots TS_{N-1}$ based on the inputs from the controller such that the transfer switches ($TS_1 \ldots TS_m$) for the m active modules connect the modules to the fuel-cell bus while the remaining $N-1-m$ transfer switches ($TS_{m+1} \ldots TS_{N-1}$) are turned off along with switches S_{m+1} through S_{N-1} for additional protection.

During the *transient state the dynamic-power-management strategy* uses any converter module that was inactive before the transient to transfer the power difference between the new load demand and the existing fuel-cell-stack input power. Thus, for an increase in the load demand, assuming m active converters were connected to the fuel-cell stack before the load transient, the power-management control system activates the remaining $N-m-1$ converters (and transfer switches $TS_{m+1} \ldots TS_{N-1}$) such that additional power is transferred from the battery to the load by equally distributing the I^*_{bat} among the $N-m-1$ converters. The reason all the $N-m-1$ converters are activated together is to have a fast dynamic response and mitigate any effect of load variation on the stack by fast battery buffering. The transient state continues until the BOPS adjusts the air-and fuel-flow rates for the fuel-cell stack for the new load demand. At that time, the net load power is again provided by the stack and the energy-efficient scheme outlined in Sec. 2.1 is applied to determine the optimal number of converter modules that need to be activated to support the new load demand. It is important to ensure the stability of the distributed PES during this structural change in the system. Therefore, in Sec. 2.2, using a recently-developed novel multiple Lyapunov approach [14], a reachability condition is outlined, which provides the condition for convergence of the PES dynamics from one steady-state condition to another.

2.1 Efficient Power-Sharing Strategy With Fuel-Cell Stack Meeting the Power Demand.

The efficiency of the jth dc-dc boost converter module is described by

$$\eta = \frac{P_{o_j}}{P_{\mathrm{in}_j}} = \frac{P_{\mathrm{in}_j} - P_{\mathrm{loss}_j}}{P_{\mathrm{in}_j}} = 1 - \frac{P_{\mathrm{loss}_j}}{P_{\mathrm{in}_j}} \tag{1}$$

where

$$P_{\mathrm{loss}_j} = P_{\mathrm{SW}_j} + P_{\mathrm{inductor}_j} + P_{\mathrm{cap}_j} + P_{\mathrm{SS}_j} + P_{\mathrm{lump}_j} \tag{2a}$$

where P_{SW_j} is the total losses in the switches of the converter, P_{inductor_j} accounts for the loss in the core and the copper loss in the inductor, P_{cap_j} is the parasitic loss in the output capacitor, P_{TS_j} is the conduction loss in the transfer switches, and P_{lump_j} corresponds to the additional losses in the converter due to the various unaccounted parasitics in the converter. The expressions for the individual losses for the dc-dc bidirectional boost converter is given by

$$P_{\mathrm{SW}_j} = f_{\mathrm{sw}}\left(\frac{2}{3}(C_{\mathrm{oss},1} + C_{\mathrm{oss},2})V_{\mathrm{bus}}^2 + \frac{1}{2}I_j V_{\mathrm{bus}} \times (t_{\mathrm{on},1} + t_{\mathrm{on},2} + t_{\mathrm{off},1} + t_{\mathrm{off},2})\right) + I_j^2\{Dr_{\mathrm{on},1} + (1-D)r_{\mathrm{on},2}\} \tag{2b}$$

$$P_{\mathrm{inductor}_j} = k_L \Delta i_j^2 f_{\mathrm{sw}} + I_j^2 r_L = k_L \frac{V_{\mathrm{in}}^2 D^2}{f_{\mathrm{sw}} L^2} + I_j^2 r_L \tag{2c}$$

$$P_{\mathrm{cap}_j} = I_{\mathrm{out}}^2 r_{\mathrm{esr}} \approx (I_j(1-D))^2 r_{\mathrm{esr}} \tag{2d}$$

$$P_{\mathrm{SS}_j} = r_{\mathrm{TS}} I_j^2 \tag{2e}$$

$$P_{\mathrm{lump}_j} = I_j^2 r_{\mathrm{para}} + C_{Lj} \tag{2f}$$

where the key parameters are defined as follows. I_j is the averaged value of module input current i_j, i.e., $I_j = \bar{i}_j$; V_{bus} is the averaged output voltage of the module, i.e., $V_{\mathrm{bus}} = \bar{v}_{\mathrm{bus}}$; V_{in} is the input voltage, which is equal to the nominal stack voltage (V_{stack}) in steady-state; D is the duty ratio of a converter module in steady-state given by $D = (V_{\mathrm{bus}} - V_{\mathrm{in}})/V_{\mathrm{bus}}$; Δi_j is the ripple in the inductor current, which is independent of the input current but depends on the input voltage of the boost converter and given by $\Delta i_j = V_{\mathrm{in}} D/(f_{\mathrm{sw}} L)$; C_{oss} is the output drain-source capacitance of the metal-oxide semiconductor field-effect transistor (MOSFET); t_{on} is the duration of turn on of the individual MOSFET; t_{off} is the duration of turn off of the individual MOSFET; r_{on} is the in resistance of the individual MOSFET; f_{sw} represents the switching frequency of the converter; r_L is the parasitic resistance of the inductor; r_{esr} is the equivalent series resistance of the capacitance; r_{para} represents the parasitic resistance of the circuit; C_{L_j} is the constant loss in the module that is independent of the power delivered by the converter; k_L is the core loss constant of the inductor; and r_{TS} represents the on resistance of the transfer switch.

Thus, it can be concluded that, for a converter operating at a particular switching frequency, the total loss is a function of I_j for a given V_{in} and V_{bus}. It is noted that, under steady-state conditions, the input voltage is the same as the voltage of the fuel-cell stack since the battery buffers the stack only under transient condition, that is, $V_{\mathrm{in}} = V_{\mathrm{stack}}$. Therefore, the steady-state efficiency of the individual stack connected converter using Eq. (1) can be modified as

$$\eta_j = \frac{P_{o_j}}{P_{\mathrm{in}_j}} = \frac{P_{\mathrm{in}_j} - P_{\mathrm{loss}_j}}{P_{\mathrm{in}_j}} = \frac{V_{\mathrm{stack}} I_j - f_j(I_j)}{V_{\mathrm{stack}} I_j} = \frac{P_{\mathrm{in}_j} - f_j(I_j)}{P_{\mathrm{in}_j}} = 1 - \frac{1}{P_{\mathrm{in}_j}} f_j(I_j) \tag{3}$$

The overall efficiency of the distributed PES (including N dc-dc modules) is given by

$$\eta = \sum_{j=1}^{m} P_{o_j} \Big/ \sum_{j=1}^{m} P_{\mathrm{in}_j} = 1 - \frac{1}{P_{\mathrm{in}}} \sum_{j=1}^{m} f_j(I_j) \tag{4}$$

where $P_{\mathrm{in}} = \Sigma_j P_{\mathrm{in}_j}$.

To maximize the efficiency of the multiconverter system with m ($\leq N-1$) number of active modules (it is noted that the Nth converter is always connected to the battery), the objective function (J_m) for a given V_{stack} is defined as

$$\mathrm{minimize}: J_m = f(I) = \sum_{j=1}^{m} f_j(I_j) \tag{5a}$$

where $j = 1, \ldots, m$ ($\leq N-1$) and $I^T = [I_1, I_2, \ldots, I_m]^T$ with the following two constraints:

$$0 \leq I_j \leq I_{\mathrm{rated}}$$

which in generic form yields

$$g_j(I) = 0 - I_j \leq 0, \quad \forall\, j = 1, \ldots, m$$

$$g_j(I) = I_j - I_{\mathrm{rated}} \leq 0, \quad \forall\, j = m+1, \ldots, 2m \tag{5b}$$

and $\Sigma_{j=1}^{m} I_j = I_{\mathrm{FC}}^* = I_{\mathrm{total}} - I_{\mathrm{bat}}^* = (V_{\mathrm{stack,oc}} - V_{\mathrm{stack}}/R_{\mathrm{ASR}})$, which in generic form yields

$$h(I) = \sum_{j=1}^{m} I_j - I_{\mathrm{FC}}^* = 0 \tag{5c}$$

It is noted that I_{bat}^* is negative when the battery is being charged. In Eqs. (5b) and (5c), I_{rated} is the current capacity of the individual converter modules, I_{total} ($= I_{\mathrm{bat}}^* + I_{\mathrm{FC}}^*$) is the current demand for a given load condition (and is less than or equal to $I_{\max}$, which is the maximum current corresponding to $P_{\max}$), $V_{\mathrm{stack,oc}}$ is the stack voltage when no current is drawn from the stack, and R_{ASR} is the equivalent resistance of the stack. Equations (5a)–(5c) represent a constrained optimization problem with both equality and inequality constraints. It is noted that, the inequality in Eq. (5b) represent a box constraint that is represented as a 2 m one-sided constraint. The Lagrangian ($L: \mathfrak{R}^m \times \mathfrak{R}^{2m} \times \mathfrak{R} \to \mathfrak{R}$) for the primal problem defined by Eqs. (5a)–(5c) is defined by

$$L(I, \lambda, v) = f(I) + \sum_{j=1}^{2m} \lambda_j g_j(I) + v h(I) \tag{6}$$

where $\lambda \in \mathfrak{R}^{2m}$ is the Lagrange multiplier (or dual variable) for the jth inequality constraint (5b), and $v \in \mathfrak{R}^1$ is the Lagrange multiplier (or dual variable) associated with the equality constraint (5c). The Lagrange dual function $w: \mathfrak{R}^{2m} \times \mathfrak{R} \to \mathfrak{R}$ corresponding to Eq. (6) is defined by [15]

$$w(\lambda, v) = \inf_{I \in \cap_{j=1}^{2m} \mathrm{dom}\, g_j(I) \cap \mathrm{dom}\, h(I)} \left(f(I) + \sum_{j=1}^{2m} \lambda_j g_j(I) + v h(I) \right)$$

and yields the lower bound on the optimal value p^* of Eq. (5) with corresponding optimal I^*. Subsequently, the optimization of this Lagrange dual function using

$$\mathrm{maximize}: w(\lambda, v) \tag{7a}$$

$$\text{subject to}: \lambda \geq 0 \tag{7b}$$

yields optimal value d^* (with corresponding dual optimal Lagrange multipliers λ^*, v^*) such that $d^* \leq p^*$, which represents the weak duality condition that always holds.

On the other hand, the strong duality condition, which is met under certain specific conditions, ensures an optimal duality gap of zero, yields $d^* = p^*$ thereby yielding optimal primal-dual operating points of (I^*, λ^*, v^*). It turns out that, if the primal problem (e.g., as described by Eq. (5)) is convex with g_j and h, respectively, convex and affine and with differentiable objective and constraint functions, the Karush–Kuhn–Tucker (KKT) condition that is outlined below yields primal and dual optimal points with zero duality gap, that is,

$$g_j(I^*) \le 0, \quad j=1,\ldots,2m \tag{8a}$$

$$h(I^*)=0 \tag{8b}$$

$$\lambda_j^* \ge 0, \quad j=1,\ldots,2m \tag{8c}$$

$$\lambda_j^* g_j(I^*)=0, \quad j=1,\ldots,2m \tag{8d}$$

$$\nabla_I L(I^*,\lambda^*,v^*)=\nabla_I f(I^*)+\sum_{j=1}^{2m}\lambda_j^*\nabla_I g_j(I^*)+v h(I^*)=0 \tag{8e}$$

An additional supplementary test for the optimal operating (I^*,λ^*,v^*) is the second-order sufficient condition, which requires that the Hessian of the Lagrangian in Eq. (6) be a positive-definite matrix, that is,

$$y^T\nabla_I^2 L(I^*,\lambda^*,v^*)y=y^T\left[\nabla_I^2 f(I^*)+\sum_{j=1}^{2m}\lambda_j^*\nabla_I g_j(I^*)+v^*\nabla_I h(I^*)\right]y > 0 \quad \forall\ y\in V(\lambda^*,v^*) \tag{8f}$$

where

$$y\in V(\lambda^*,v^*)\Leftrightarrow\left\{\begin{matrix}\nabla g_j(I^*)^T y=0, & \forall j=1,\cdots,2m\\ \nabla h(I^*)^T y=0 & \end{matrix}\right\} \tag{8g}$$

The solution to the optimization problem in Eq. (5) determines the optimal distribution of the input currents among the m dc-dc converters. The overall system objective is to find the number of modules to be connected (i.e., m^*) such that the cost function J_m as defined in Eq. (5a) is minimized, that is, $m^* = \arg\min_{\frac{I_{\text{total}}}{I_{\text{rated}}}\le m\le N-1}\{J_m\}$.

2.1.1 A Case Illustration With $m=3$. Following Eqs. (2b)–(2f), we express Eq. (5a) as

$$\text{minimize:}J_m=f(I)=\sum_{j=1}^{3}f_j(I_j)=\sum_{j=1}^{3}\alpha_j I_j^2+\beta_j I_j+\gamma_j, \quad \forall\ \alpha_j > 0,\beta_j>0,\gamma_j>0 \tag{9}$$

with the constraints described by Eqs. (5b) and (5c) for $m=3$. In Eq. (9), coefficients α_j, β_j, and γ_j can be determined based on power-stage parameters or can be determined by experimentally mapping the loss function of the jth module $f_j(I_j)$ as a function of the input current. Using the Lagrangian in Eq. (6) to the primal problem defined by Eqs. (9), (5b), and (5c), and following Eq. (9), the KKT optimality conditions described by

$$g_j(I^*)=0-I_j^*\le 0, \quad \forall j=1,\ldots,3 \quad \text{and} \quad g_j(I^*)=I_j^*-I_{\text{rated}} \le 0, \quad \forall j=4,\ldots,6 \tag{10a}$$

$$h(I^*)=I_1^*+I_2^*+I_3^*-I_{\text{FC}}^*=0 \tag{10b}$$

$$\lambda_j^*\ge 0, \quad j=1,\ldots,6 \tag{10c}$$

$$\lambda_j^* g_j(I^*)=\lambda_j^*(0-I_j^*)\le 0, \quad \forall j=1,\ldots,3 \quad \text{and} \quad g_j(I^*)=\lambda_j^*(I_j^* - I_{\text{rated}})\le 0, \quad \forall j=4,\ldots,6 \tag{10d}$$

$$\nabla_I L(I^*,\lambda^*,v)=\begin{pmatrix}2\alpha_1&0&0\\0&2\alpha_2&0\\0&0&2\alpha_3\end{pmatrix}\begin{pmatrix}I_1^*\\I_2^*\\I_3^*\end{pmatrix}+\begin{pmatrix}\beta_1\\\beta_2\\\beta_3\end{pmatrix}+\lambda_1^*\begin{pmatrix}-1\\0\\0\end{pmatrix}+\lambda_2^*\begin{pmatrix}0\\-1\\0\end{pmatrix}+\lambda_3^*\begin{pmatrix}0\\0\\-1\end{pmatrix}+\lambda_4^*\begin{pmatrix}1\\0\\0\end{pmatrix}+\lambda_5^*\begin{pmatrix}0\\1\\0\end{pmatrix}+\lambda_6^*\begin{pmatrix}0\\0\\1\end{pmatrix}+v^*\begin{pmatrix}1\\1\\1\end{pmatrix}=\begin{pmatrix}0\\0\\0\end{pmatrix} \tag{10e}$$

Equations (10a)–(10e) are satisfied only when

$$\lambda_j^*=0(\forall j=1,\ldots,6) \tag{11}$$

Thus, Eq. (10e) simplifies to

$$\begin{pmatrix}2\alpha_1 I_1^*+\beta_1\\2\alpha_2 I_2^*+\beta_2\\2\alpha_3 I_3^*+\beta_3\end{pmatrix}+v^*\begin{pmatrix}1\\1\\1\end{pmatrix}=\begin{pmatrix}0\\0\\0\end{pmatrix} \tag{12}$$

Using Eqs. (12) and (10b), we obtain the optimal solutions for I^* to be

$$v^*=-\left(I_{\text{FC}}^*+\sum_{j=1}^{3}\frac{\beta_j}{2\alpha_j}\right)\left(\sum_{j=1}^{3}\frac{1}{2\alpha_j}\right)^{-1}, \quad \forall j=1,\ldots,3 \tag{13}$$

$$I_j^*=-\frac{1}{2\alpha_j}\left(-\left(I_{\text{total}}+\sum_{j=1}^{3}\frac{\beta_j}{2\alpha_j}\right)\left(\sum_{j=1}^{3}\frac{1}{2\alpha_j}\right)^{-1}+\beta_j\right), \quad \forall j=1,\ldots,3 \tag{14}$$

For the special case, when all the converter modules have identical parameters (i.e., $\alpha_1=\alpha_2=\alpha_3=\alpha$ and $\beta_1=\beta_2=\beta_3=\beta$), Eqs. (13) and (14) reduce to the following:

$$v^*=-\left(\tfrac{\alpha}{2}I_{\text{total}}+\beta\right), \quad \forall j=1,\ldots,3 \tag{15}$$

$$I_j^*=\frac{1}{3}I_{\text{total}}, \quad \forall j=1,\ldots,3 \tag{16}$$

Furthermore, the Hessian of the Lagrangian in Eq. (10e) yields

$$\nabla_I^2 L(I^*,\lambda^*,v^*)=\begin{pmatrix}2\alpha_1&0&0\\0&2\alpha_2&0\\0&0&2\alpha_3\end{pmatrix} \tag{17}$$

which is a positive-definite matrix given that $\alpha_1>0$, $\alpha_2>0$, and $\alpha_3>0$. *Therefore, the optimality condition* (for $N>1$) is expected to be achieved when the connected m dc-dc converters share the current equally among them.

2.2 Reaching Criterion for Post-Load-Transient Stability Analysis With Fuel-Cell Stack and Battery Meeting the Power Demand. While Sec. 2.1 outlines the issue of optimal power management under steady-state conditions for different load demands, an issue of equal importance is ensuring the transient stability of the distributed PES when the number of converter modules may change following a variation in the power demand of the application load. Conventional stability analyses of PES using average models or nonlinear maps assume orbital existence [16]. However for global stability, convergence of the reaching dynamics of the PES to its orbit for a given initial condition is essential. Therefore, reaching criterion based analysis [14] of the distributed PES is needed to ensure its post-transient stability, as outlined below.

To obtain the reaching condition, first, the distributed PES is described by the following piecewise linear (PWL) state-space equation:

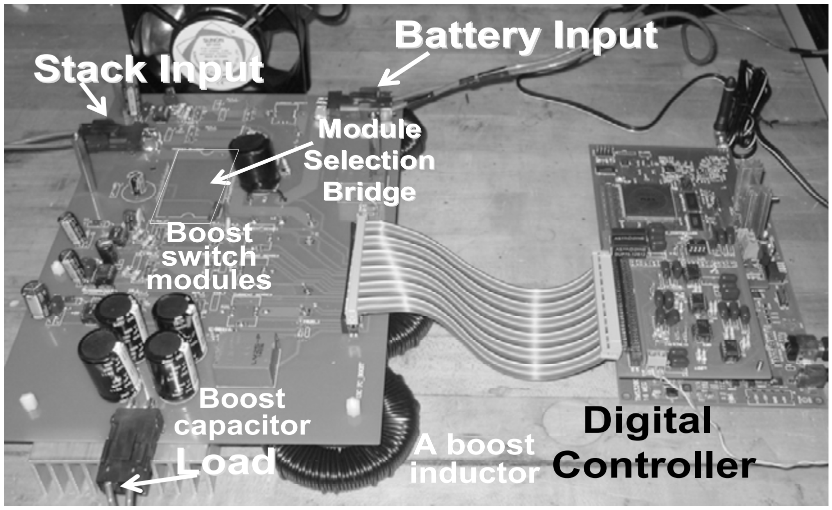

(a)

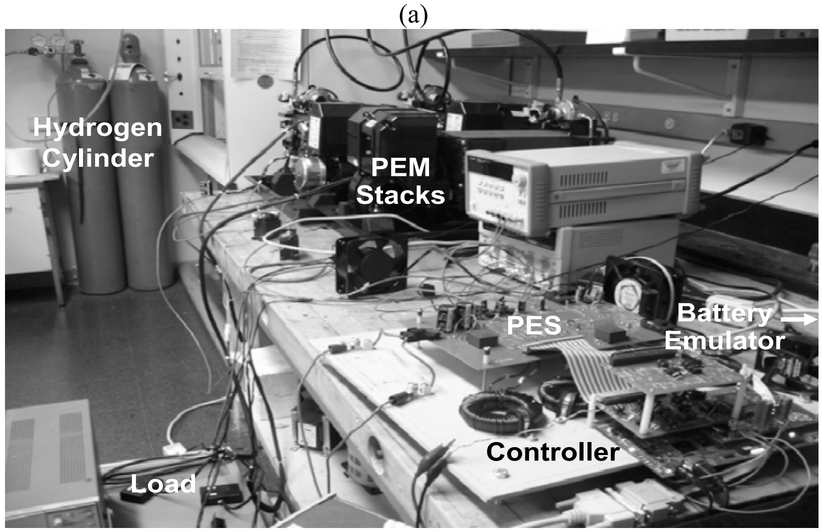

(b)

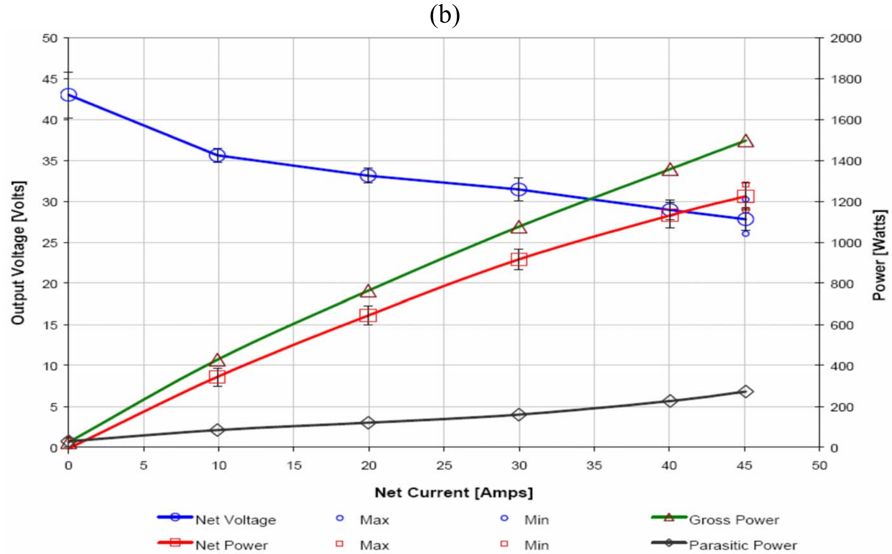

Fig. 3 Experimental prototype of the (*a*) distributed PES and (*b*) a setup for the overall (two-stack) PEM fuel-cell based power system. (*c*) The polarization curve (*source: Nexa technical specifications*) for each PEM stack.

Table 1 Nominal PES module parameters

Boost inductance=1 mH	$C_{\mathrm{oss},1}=9.4$ nF	$t_{\mathrm{off},2}=220$ ns	$C_L=8.4$ W	$R_{\mathrm{ASR}}=0.8$
Switching frequency=20 kHz	$C_{\mathrm{oss},2}=880$ pF	$r_{\mathrm{on},1}=100$ mΩ	$K_v=2\times 10^5$	$V_{\mathrm{stack,oc}}=43.5$ V (for each stack)
Rated power=700 W	$r_L=60$ mΩ	$r_{\mathrm{on},2}=110$ mΩ	$\omega_{zv}=700$ rad/s	R(nominal value)=21.5 Ω
Bus capacitance=440 μF	$k_L=4\times 10^{-6}$	$r_{\mathrm{SS}}=75$ mΩ		$\omega_{pv}=3.1\times 10^4$ rad/s
Input voltage=55–70 V	$t_{\mathrm{on},1}=110$ ns	$r_{\mathrm{esr}}=11$ mΩ		$K_i=7.5\times 10^4$
On resistance of transfer switch=13 mΩ	$t_{\mathrm{off},1}=220$ ns	$t_{\mathrm{off},2}=220$ ns		$\omega_{zi}=800$ rad/s
Bus voltage=120 V	$t_{\mathrm{on},2}=140$ ns	$r_{\mathrm{para}}=100$ mΩ		$\omega_{pi}=3.2\times 10^4$ rad/s

$$\dot{x}(t) = A_i x(t) + B_i \tag{18}$$

where i is an integer that represents the switching states of the PES, $x(t)\in\Re^n$ represent the states of the PES, $A_i\in\Re^{n\times n}$ are the matrices, and $B_i\in\Re^n$ are the column vectors for each of the switching states of the PES. The Appendix provides two case illustrations on the derivation of the matrices A_i and B_i for a closed-loop PES operating with $m=2$ and $m=3$ active modules after the transient. Now, dropping the notation of time (here on) and translating Eq. (18) into error coordinates using $e=x-x^*$, where e represents the error vector and x^* represents the vector of steady-state values of the states of the PES, Eq. (18) can be rewritten as

$$\dot{e} = A_i e + A_i x^* + B_i = A_i e + \bar{B}_i \tag{19}$$

where $\bar{B}_i=B_i+A_i x^*$. Subsequently, to determine the reaching criterion of the PES, a convex combination of multiple positive-definite and quadratic Lyapunov functions, $V_k(e)>0$ (for the kth switching sequence) is defined as follows:

$$V_k(e) = \sum_{i=1}^{h} \alpha_{ki} e^T P_{ki} e, \quad \forall\, k=1,2,\ldots,M \tag{20}$$

In Eq. (20), for continuous-conduction-mode operation of the dc-dc converters, $M=\Sigma_{l=1}^{(2^N-W)}\binom{2^N-W}{l}$ [14] is the total number of possible switching sequences of the PES with N and W being the total number of noncomplementary switching functions and the number of redundant switching states, respectively. Furthermore, h is the number of switching states in a given sequence, $0\le\alpha_{ki}\le 1$, $\sum_{i=1}^{h}\alpha_{ki}=1$, and $P_{ki}=P_{ki}^T$ is a positive-definite matrix (i.e., all of its eigenvalues are positive and hence, the minimum eigenvalue of P_{ki} is greater than zero [17]. Now, according to Lyapunov's criterion, the trajectories of the PES described by Eq. (19) converge toward the orbit for finite switching frequency provided that

$$\dot{V}_k(e) = \sum_{i=1}^{h} \alpha_{ki}(\dot{e}^T P_{ki} e + e^T P_{ki}\dot{e}) < 0 \tag{21}$$

Using Eqs. (19) and (20), Eq. (21) can be transformed to the following:

$$\frac{d}{dt}V_k(e) = \sum_{i=1}^{h} \alpha_{ki} \begin{bmatrix} e \\ 1 \end{bmatrix}^T \begin{bmatrix} A_i^T P_{ki} + P_{ki} A_i & P_{ki}\bar{B}_i \\ \bar{B}_i^T P_{ki} & 0 \end{bmatrix} \begin{bmatrix} e \\ 1 \end{bmatrix} < 0 \tag{22}$$

which implies that

$$\sum_{i=1}^{h} \alpha_{ki} \begin{bmatrix} A_i^T P_{ki} + P_{ki} A_i & P_{ki}\bar{B}_i \\ \bar{B}_i^T P_{ki} & 0 \end{bmatrix} < 0 \tag{23}$$

Now, because $0\le\alpha_{ki}\le 1$, $\Sigma_{i=1}^{h}\alpha_{ki}=1$, the matrix inequality in Eq. (23) can be represented as a conventional convex optimization problem with linear-matrix-inequality constraints. This convex optimization problem is of the class of feasibility problems, which involves obtaining a matrix P_{ki} such that the linear-matrix-inequality in Eq. (23) is satisfied. These problems can be solved by using computationally efficient interior-point algorithms [18] and are available in common mathematical tools like MATLAB. However, if there are no solutions of P_{ki} for Eq. (23) (which is automatically indicated in MATLAB when the total number of iterations exceed a default threshold), the dual of $V_k(e)$ is investigated to confirm that the state error trajectories of the PES states do not converge to the orbit. In that case, one needs to find the dual of $V_k(e)$, which is defined as

$$V_{Dk}(e) = \sum_{i=1}^{h} \lambda_{ki} e^T Q_{ki} e \tag{24}$$

where $0\le\lambda_{ki}\le 1$, $\Sigma_{i=1}^{h}\lambda_{ki}=1$, $Q_{ki}=Q_{ki}^T$ is a positive-definite matrix. To confirm that the state-error trajectories of the PES do not converge to the orbit for the kth switching sequence, $V_{Dk}(e)$ has to satisfy the following criteria:

$$V_{Dk}(e) > 0 \quad \text{and} \quad \frac{d}{dt}V_{Dk}(e) > 0 \tag{25}$$

or

$$-V_{Dk}(e) = \sum_{i=1}^{h} \lambda_{ki} e^T(-Q_{ki}) e < 0 \quad \text{and} \quad -\frac{d}{dt}V_{Dk}(e) < 0 \tag{26}$$

Following Eqs. (20) and (21), Eq. (26) can be reduced similar to Eq. (23) to the following form for the dual condition:

$$\sum_{i=1}^{h} \lambda_{ki} \begin{bmatrix} -A_i^T Q_{ki} - Q_{ki} A_i & -Q_{ki}\bar{B}_i \\ -\bar{B}_i^T Q_{ki} & 0 \end{bmatrix} < 0 \tag{27}$$

If there are no solutions of P_{ki} for Eq. (23) but there exist solutions of Q_{ki} for Eq. (27), the state-error trajectories of the PES do not converge to an orbit, which implies that after a load transient, the PES dynamics will not converge to the new steady-state.

3 PES Prototype Design and Results

The PES power stage for the distributed hybrid power system prototype is designed with four bidirectional dc-dc boost converters (i.e., $N=4$), for a 2 kW application, with each module rated for 700 W with a rated current of 14 A. The input voltage range is chosen as 55–70 V. The regulated output dc bus voltage of the PES is 120 V. The switching frequency of the boost converters is chosen to be 20 kHz. Figure 3(a) shows the experimental distributed PES with parameters provided in Table 1. The design is implemented using two boards: one for the power stage and the other for the controller. The controller interface receives the current- and voltage-sense feedback signals from the power board using a multistrand cable and provides the switching signals for the converter modules and the transfer switches using the same interface. A spectrum digital DSK TMS3206713 along with a high-speed Altera FPGA (EPF10K50VRC240-2) is used for implementing the compensators and generating the digital control signals for the converter switches and the transfer switches. To deactivate a particular bidirectional converter, both the switches

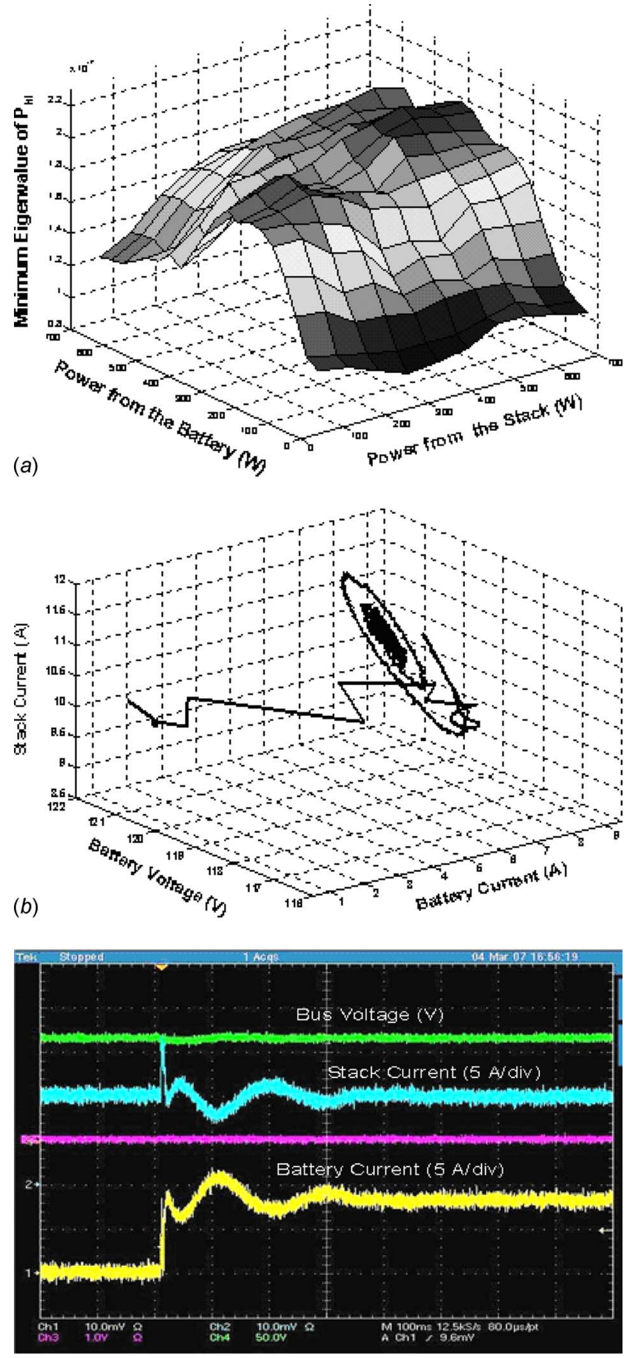

Fig. 4 Post-transient stability of the distributed PES after a load transient from 0.6 kW to 1 kW. Initially one module feeds the load from the stack, and subsequently after the transient, a second module is activated that feeds the additional power from the battery. (*a*) Minimum eigenvalue of $P_{ki}>0$ implies that positive P_{ki} is positive definite and that reaching condition (23) is satisfied for all initial power demand for $m=2$, thereby ensuring convergence of PES dynamics after the second module is activated following the load transient. ((*b*) and (*c*)) Experimental validations of reachability and stabilization of the currents.

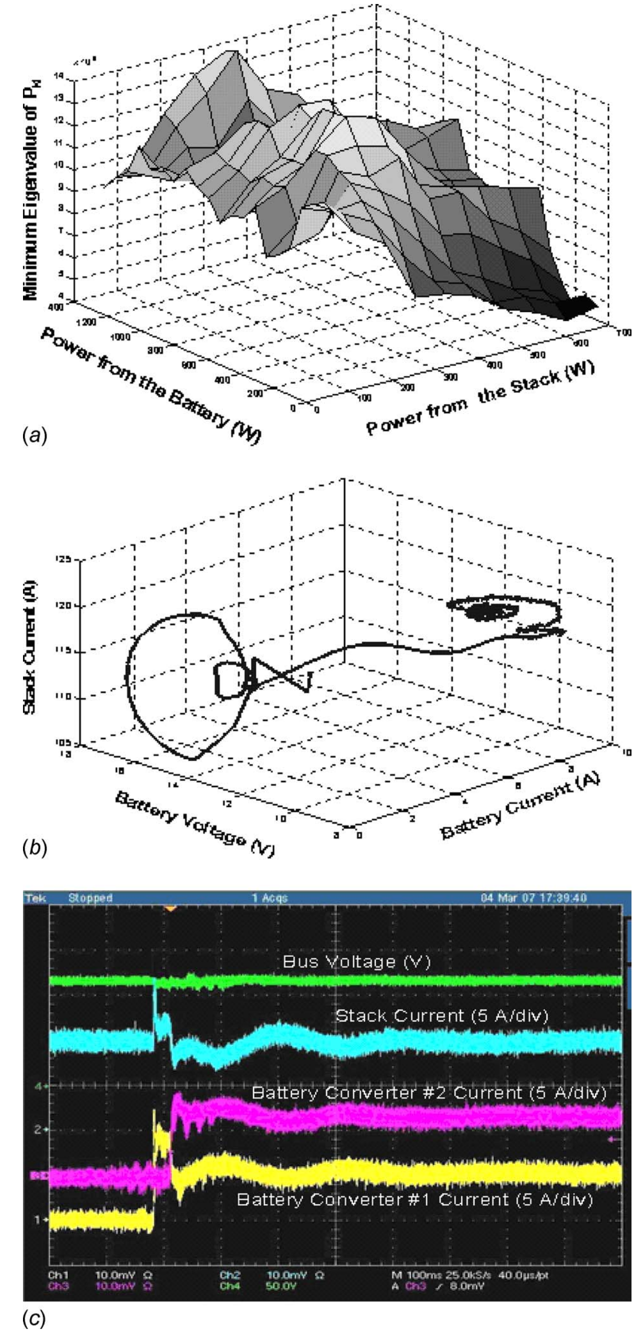

Fig. 5 Post-transient stability of the distributed PES after a load transient from 0.6 kW to 1.4 kW. Initially one module feeds the load from the stack, and subsequently after the transient, two modules are activated that feeds the additional power from the battery. (*a*) Minimum eigenvalue of $P_{ki}>0$ implies that positive P_{ki} is positive definite and that reaching condition (23) is satisfied for all initial power demand for $m=3$, thereby ensuring convergence of PES dynamics after the second module is activated following the load transient. ((*b*) and (*c*)) Experimental validations of reachability and stabilization of the currents.

need to be turned off simultaneously and hence, control signal of each of the switches are generated using the high-speed IR2103 [20] that provides very efficient cross-conduction prevention logic. Regarding the transfer switches, since they undergo turn on and turn off much less frequently compared with the converter switches, their switching losses are negligible. However, they need to have very small on resistance (r_{ds_ON}) to reduce their conduction losses. As such, a three-phase MOSFET bridge MSK 4401 [19] with integrated gate drive is used to activate/deactivate the converter modules. The on resistance of each of the transfer switches in the bridge is only 13 mΩ, which yields a maximum loss of 2.5 W even at full load. Using the experimental PES, we

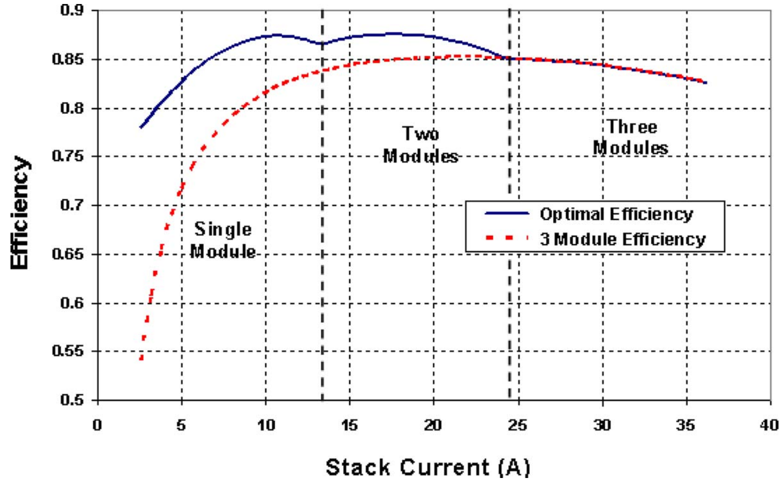

Fig. 6 Experimental comparison of the PES efficiency with varying stack current level. (top trace) Efficiency when *m* is varied between 1 through 3 following the optimal criterion outlined in Sec. 2.1. When $m=2$ or $m=3$, the current is shared equally among the modules. (bottom trace) Efficiency when *m* is always 3 (i.e., no optimal power management implemented) and all the modules share current equally. Clearly, the former demonstrates flatter efficiency profile of the PES leading to better fuel-cell-stack utilization in steady-state.

now evaluate the transient stability and optimal steady-state performance of the PES, following the methodology described in Secs. 2.2 and 2.1, respectively.

To test whether the dynamics of the distributed PES converges in the presence of a load transient, we demonstrate a twofold validation. First, using the reaching condition outlined in Eq. (23), we evaluate the post-transient stability of the PES for a given m. This is ascertained by plotting the minimum eigenvalue of P_{ki}, which if positive proves that the post-transient PES dynamics will converge to the equilibrium for any arbitrary initial condition. Subsequently, we conduct experimental validation of convergence of PES dynamics in parametric and time domains after the transient. Figure 4(*c*) illustrates the transient stability of the PES (for $N=3$ and $m \leq N-1$) when the load demand varies from 0.6 kW to 1 kW. Before the transient, only one converter feeds the load from the fuel-cell stack. However, immediately after the transient, the other available converter for transient condition is activated, which ensures that while the stack current remains at the pretransient level, the battery picks up the additional current. Figure 4(*b*) illustrates the convergence of the post-load-transient dynamics in parametric domain. The initial oscillations in the battery and the stack currents are due to the interaction between the two converters. Figure 4(*a*) demonstrates the generalized results based on the reaching condition (23) for a resistive load with modules sharing current equally and having the same nominal parameters. It shows that the minimum eigenvalue of P_{ki} in Eq. (23) is greater than zero, thereby establishing that P_{ki} is positive definite and implying that for $m=2$ the dynamics of the distributed PES will converge to the equilibrium for all initial power demand. In other words, following the load transient when the two modules are activated, the system dynamics will stabilize (for arbitrary initial condition) since the reaching condition is satisfied. Along the same lines as above, Figs. 5(*a*)–5(*c*) provide stability results for the load transient (0.6 kW$\rightarrow$1.4 kW). However, in this scenario, following the load transient, two additional modules are activated instead of one for the previous case. Thus, after the transient of the three modules ($m=3$), one module continues to provide the (pretransient-level) power from the stack while the two converters activated after the transient provide the additional power from the battery. We note that the second battery converter is activated 20 ms after the first, and this is attributed to the dynamics of the reference battery current and the slight discrepancy of the two current references due to slight mismatch among the power-stage parameters of the two converter modules.

However, after this initial time lag, the converters share the current equally among them. Overall, post-transient stability is achieved and experimental results and reaching-condition prediction are in harmony.

With regard to the optimal performance in the equilibrium condition outlined in Sec. 2.1, Fig. 6 shows the improvement in the PES efficiency (demonstrated by the top trace) when the number of active modules is varied (from one through three) as a function of the stack current compared with when three equal-current-sharing modules are always activated. Clearly, using the optimal number of PES modules flattens efficiency over a larger power range [13]. This is achieved because as the load demand drops and so does the stack current requirement, without power management, the efficiency of the PES when it is always operated with three (equal-current-sharing) active modules drops; however, when power management is implemented, the control system determines the optimal number of modules needed for a given load demand and yet maximize the efficiency. This is because reducing the number of active modules pushes the power requirement from the remaining modules, thereby yielding higher efficiency since typically converters yield the highest efficiency near their rated output power.

4 Conclusions

A power-management control system based on distributed PES for a fuel-cell based energy system is outlined. Unlike the conventional approach, which typically uses a lumped PES unit for interfacing the stack to the application load, the distributed PES has multiple modules, which can be controlled and selectively activated depending on the load demand. Of the N distributed modules, up to $N-1$ can be connected to the fuel-cell-stack or the battery under steady-state or transient condition, while the Nth converter is connected to the battery for charging even under full-load condition. For part-load operation, additional modules can be used for battery charging as well. Thus, the need for a dedicated full-power-rating battery converter (as in conventional approach) is significantly minimized. As the load demand increases, an optimal criterion determines the number of such modules that need to be activated for maximum PES energy-conversion efficiency that, in return, leads to enhanced stack utilization. This optimal criterion has been developed using a convex optimization framework. Although this paper outlines an analytical formulation of the optimization function (representing the overall loss of the PES), the coefficients for the optimization function can be determined experimentally as well by simply mapping the loss (with varying power demands) as a function of the input current. Furthermore, since the power-management scheme relies on the selection of the optimal number of active modules following the change in load demand, a reaching criterion has been developed to ensure the post-load-transient stability of the PES. The reaching criterion uses a multiple-Lyapunov-function based methodology and determination of the convergence of PES dynamics simply requires solving a matrix inequality. Predictions of both the optimal criterion and the reaching criterion have been validated. The results show that the optimal power management strategy leads to flatter and to a higher efficiency of the PES for most part along with convergence of the post-load-transient PES dynamics for varying load conditions. Overall, the distributed-PES-based power-management-control scheme leads to enhanced source utilization due to better PES efficiency profile and reduces (as compared totypical conventional approach) the requirements of footprint space, weight, and cost for battery buffering by significantly reducing the requirement for a dedicated full-power-rating converter for the battery.

Acknowledgment

This paper is prepared with the support of the U.S. Environmental Protection Agency (EPA) and U.S. Department of Energy (DOE) under Award Nos. RD-83158101-0 and DE-FC2602NT41574, respectively. This work was also supported in part by the National Science Foundation (NSF) CAREER Award received by Professor Mazumder in the year 2003 under Award No. 0239131.

Appendix

When two bidirectional modules of the PES are active (i.e., $m=2$) the corresponding matrices are derived as

$$A_i = \begin{bmatrix} \multicolumn{3}{c}{A_{\mathrm{II}}} & & & \multicolumn{4}{c}{0_{3\times 6}} \\ 0 & 0 & -1 & -\omega_{pv} & 0 & 0 & 0 & 0 & 0 \\ 0 & 0 & 0 & 1 & 0 & 0 & 0 & 0 & 0 \\ -1 & 0 & 0 & a_1K_v & a_1K_v\omega_{zv} & -\omega_{pi1} & 0 & 0 & 0 \\ 0 & 0 & 0 & 0 & 0 & 1 & 0 & 0 & 0 \\ 0 & -1 & 0 & a_2K_v & a_2K_v\omega_{zv} & 0 & 0 & -\omega_{pi2} & 0 \\ 0 & 0 & 0 & 0 & 0 & 0 & 0 & 1 & 0 \end{bmatrix} \quad \text{and} \quad B_i = \begin{bmatrix} B_{\mathrm{II}} \\ V_{\mathrm{bus}}^{*} \\ 0 \\ 0 \\ 0 \\ 0 \\ 0 \end{bmatrix} \tag{A1}$$

where a_1 and a_2 are fraction of the total current shared by each of the individual boost converter module, K_v, ω_{zv}, and ω_{pv} are the gain, location of zero and location of the pole for the voltage loop, respectively, ω_{pi1} and ω_{pi2} are the location of the poles for the two converters. The matrices A_{II} and B_{II} are given as

$$A_{\mathrm{II}} = \begin{bmatrix} -\dfrac{1}{L_1}\left[r_{L_1} + \dfrac{\bar{S}_1 R r_C}{R+r_C} + k_{\mathrm{FC1}}R_{\mathrm{ASR}}\right] & -\dfrac{1}{L_1}\dfrac{\bar{S}_2 R r_C}{R+r_C} & -\dfrac{\bar{S}_1 R}{L_1(R+r_C)} \\ -\dfrac{1}{L_2}\dfrac{\bar{S}_1 R r_C}{R+r_C} & -\dfrac{1}{L_2}\left[r_{L_2} + \dfrac{\bar{S}_2 R r_C}{R+r_C} + k_{\mathrm{FC2}}R_{\mathrm{ASR}}\right] & -\dfrac{\bar{S}_2 R}{L_2(R+r_C)} \\ \dfrac{1}{C}\dfrac{\bar{S}_1 R}{(R+r_C)} & \dfrac{1}{C}\dfrac{\bar{S}_2 R}{(R+r_C)} & -\dfrac{1}{C}\dfrac{1}{R+r_C} \end{bmatrix}$$

$$B_{\mathrm{II}} = \left[\frac{k_{\mathrm{FC1}}V_{\mathrm{stack,oc}} + (1-k_{\mathrm{FC1}})V_{\mathrm{bat}}^{*}}{L_1} \quad \frac{k_{\mathrm{FC2}}V_{\mathrm{stack,oc}} + (1-k_{\mathrm{FC2}})V_{\mathrm{bat}}^{*}}{L_2} \quad 0\right]^T \tag{A2}$$

where k_{FC} is a constant, which indicates whether the converter is connected to the stack (=1) or the battery (=0). On a similar note, for three active bidirectional modules (i.e., $m=3$), the corresponding matrices are derived as

$$A_i = \begin{bmatrix} \multicolumn{4}{c}{A_{\mathrm{III}}} & & & \multicolumn{6}{c}{0_{4\times 8}} \\ 0 & 0 & 0 & -1 & -\omega_{pv} & 0 & 0 & 0 & 0 & 0 & 0 & 0 \\ 0 & 0 & 0 & 0 & 1 & 0 & 0 & 0 & 0 & 0 & 0 & 0 \\ -1 & 0 & 0 & 0 & a_1K_v & a_1K_v\omega_{zv} & -\omega_{pi1} & 0 & 0 & 0 & 0 & 0 \\ 0 & 0 & 0 & 0 & 0 & 0 & 1 & 0 & 0 & 0 & 0 & 0 \\ 0 & -1 & 0 & 0 & a_2K_v & a_2K_v\omega_{zv} & 0 & 0 & -\omega_{pi2} & 0 & 0 & 0 \\ 0 & 0 & 0 & 0 & 0 & 0 & 0 & 0 & 1 & 0 & 0 & 0 \\ 0 & 0 & -1 & 0 & a_3K_v & a_3K_v\omega_{zv} & 0 & 0 & 0 & 0 & -\omega_{pi3} & 0 \\ 0 & 0 & 0 & 0 & 0 & 0 & 0 & 0 & 0 & 0 & 1 & 0 \end{bmatrix} \quad \text{and} \quad B_i = \begin{bmatrix} B_{\mathrm{III}} \\ V_{\mathrm{bus}}^{*} \\ 0 \\ 0 \\ 0 \\ 0 \\ 0 \\ 0 \\ 0 \end{bmatrix} \tag{A3}$$

where a_1 and a_2 and a_3 are fractions of the total current shared by each of the individual boost converter module and

$$A_{\mathrm{III}} = \begin{bmatrix} -\frac{1}{L_1}\left[r_{L_1} + \frac{\bar{S}_1 R r_C}{R+r_C} + k_{\mathrm{FC1}}R_{\mathrm{ASR}}\right] & -\frac{1}{L_1}\frac{\bar{S}_2 R r_C}{R+r_C} & -\frac{1}{L_1}\frac{\bar{S}_3 R r_C}{R+r_C} & -\frac{\bar{S}_1 R}{L_1(R+r_C)} \\ -\frac{1}{L_2}\frac{\bar{S}_1 R r_C}{R+r_C} & -\frac{1}{L_2}\left[r_{L_2} + \frac{\bar{S}_2 R r_C}{R+r_C} + k_{\mathrm{FC2}}R_{\mathrm{ASR}}\right] & -\frac{1}{L_2}\frac{\bar{S}_3 R r_C}{R+r_C} & -\frac{\bar{S}_2 R}{L_2(R+r_C)} \\ -\frac{1}{L_3}\frac{\bar{S}_1 R r_C}{R+r_C} & -\frac{1}{L_3}\frac{\bar{S}_2 R r_C}{R+r_C} & -\frac{1}{L_3}\left[r_{L_3} + \frac{\bar{S}_3 R r_C}{R+r_C} + k_{\mathrm{FC3}}R_{\mathrm{ASR}}\right] & -\frac{\bar{S}_3 R}{L_3(R+r_C)} \\ \frac{1}{C}\frac{\bar{S}_1 R}{(R+r_C)} & \frac{1}{C}\frac{\bar{S}_2 R}{(R+r_C)} & \frac{1}{C}\frac{\bar{S}_3 R}{R+r_C} & -\frac{1}{C}\frac{1}{R+r_C} \end{bmatrix}$$

$$B_{\mathrm{III}} = \begin{bmatrix} \frac{k_{\mathrm{FC1}}V_{\mathrm{stack,oc}} + (1-k_{\mathrm{FC1}})V^*_{\mathrm{bat}}}{L_1} & \frac{k_{\mathrm{FC2}}V_{\mathrm{stack,oc}} + (1-k_{\mathrm{FC2}})V^*_{\mathrm{bat}}}{L_2} & \frac{k_{\mathrm{FC3}}V_{\mathrm{stack,oc}} + (1-k_{\mathrm{FC3}})V^*_{\mathrm{bat}}}{L_3} & 0 \end{bmatrix} \tag{A4}$$

References

[1] Achenbach, E. A., 1995, "Response of a Solid Oxide Fuel Cell to Load Change," J. Power Sources, **57**, pp. 105–109.

[2] Gemmen, R., 2003, "Analysis for the Effect of Inverter Ripple Current on Fuel Cell Operating Condition," ASME J. Fluids Eng., **125**(3), pp. 576–585.

[3] Mazumder, S. K., Pradhan, S., Hartvigsen, J., Rancruel, D., and von Spakovsky, M. R., 2007, "Investigation of Load-Transient Mitigation Techniques for Planar Solid-Oxide Fuel Cell (PSOFC) Power-Conditioning Systems," IEEE Trans. Energy Convers., **22**(2), pp. 457–466.

[4] Pradhan, S., Mazumder, S. K., Hartvigsen, J., and Hollist, M., 2007, "Effects of Electrical Feedbacks on Planar Solid-Oxide Fuel Cell," ASME J. Fuel Cell Sci. Technol., **4**(2), pp. 154–166.

[5] Hsiao, Y. C., and Selma, J. R., 1997, "The Degradation of SOFC Electrodes," Solid State Ionics, **98**, pp. 33–38.

[6] Hochgraph, C., and Singh, P., 2004, "Method and System for Fuel Cell Control," U.S. Patent 6,794,844.

[7] Early, J., and Werth, J., 1990, "Fuel Cell/Battery Control System," U.S. Patent 4,961,151.

[8] Jossen, A., Garche, J., Doering, H., Goetz, M., Knaupp, W., and Joerissen, L., 2005, "Hybrid Systems With Lead–Acid Battery and Proton-Exchange Membrane Fuel Cell," J. Power Sources, **144**, pp. 395–401.

[9] Gao, L., Jiang, Z., and Dougal, R. A., 2005, "Evaluation of Active Hybrid Fuel Cell/Battery Power Sources," IEEE Trans. Aerosp. Electron. Syst., **41**(1), pp. 346–355.

[10] Droppo, G. W., Schienbein, L. A., Harris, B. E., and Hammerstorm, D. J., 2003, "DC to DC Converter and Power Management System," U.S. Patent 6,628, 011.

[11] Jang, S. J., Lee, T. W., Lee, W. C., and Won, C. Y., 2004, "Bi-Directional DC-DC Converter for Fuel Cell Generation System," IEEE Power Electronics Specialists Conference, Vol. 6, pp. 4722–4728.

[12] Kambouris, C. A., and Bates, J. T., 2006, "DC-DC Converter for a Fuel Cell System," U.S. Patent 7014,928,B2.

[13] Pradhan, S., 2007, "Modeling, Analysis and Control of Effects of the Electrical Feedbacks on PSOFC Power Conditioning System," Ph.D. thesis, University of Illinois at Chicago, Chicago, IL.

[14] Mazumder, S. K., and Acharya, K., 2006, "Multiple Lyapunov Function Based Reaching Condition Analyses of Switching Power Converters," IEEE Power Electronics Specialists Conference, pp. 2232–2239.

[15] Boyd, S., and Vandenberghe, L., 2004, *Convex Optimization*, Cambridge University Press, New York.

[16] Mazumder, S. K., Nayfeh, A. H., and Boroyevich, D., 2001, "Theoretical and Experimental Investigation of the Fast- and Slow-Scale Instabilities of a DC/DC Converter," IEEE Trans. Power Electron., **16**(2), pp. 201–216.

[17] Brogan, W. L., 1990, *Modern Control Theory*, Prentice-Hall, Upper Saddle River, NJ.

[18] Nesterov, Y., and Nemirovskii, A., 1995, "An Interior-Point Method for Generalized Linear-Fractional Problems," Math. Program. Ser. B, **69**(1), pp. 177–204.

[19] M.S. Kennedy Corporation, MSK 4401 datasheet, http://www.mskennedy.com/client_images/catalog19680/pages/files/4401re.pdf.

[20] International Rectifier, IR2103 datasheet, www.irf.com/product-info/datasheets/data/ir2103.pdf.